AD-A080 574 FAIRCHILD CAMERA AND INSTRUMENT CORP PALO ALTO CALIF --ETC F/G 20/12
STRUCTURAL AND ELECTRICAL INVESTIGATION OF THE SI-SIO2 INTERFAC--ETC(U)
OCT 79 B E DEAL, R R RAZOUK DAAG29-78-C-0033

UNCLASSIFIED ARO-16245.3-A-EL NL

| OF |
AD
A080574

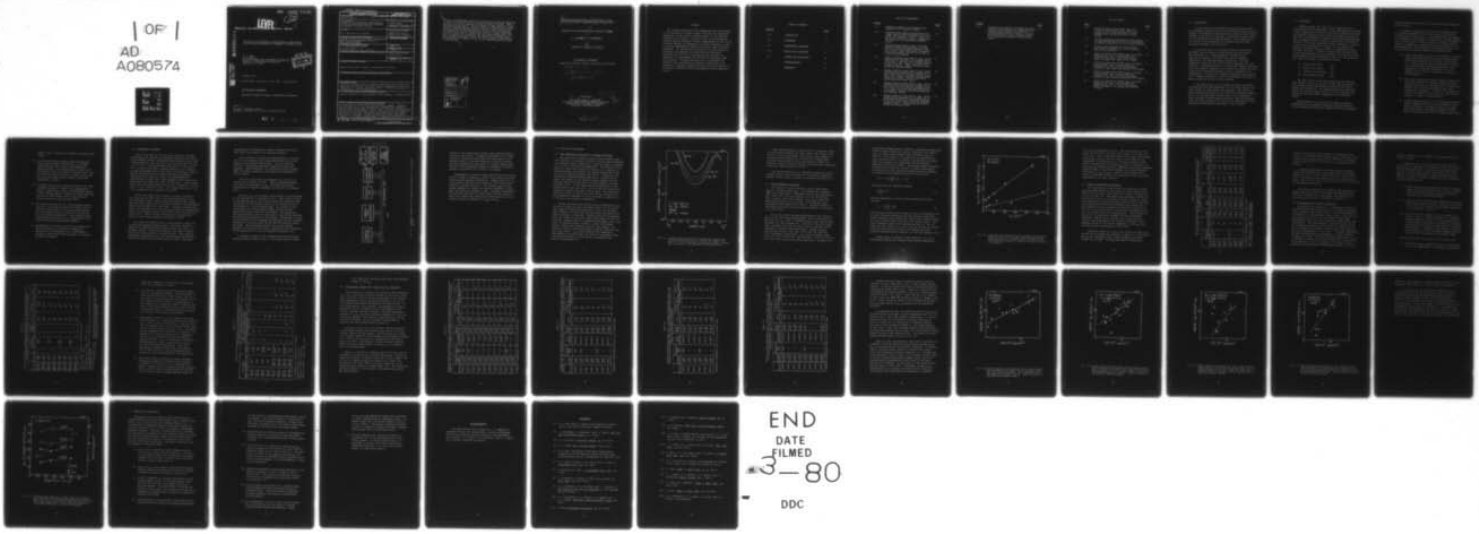

END
DATE
FILMED
3-80
DDC

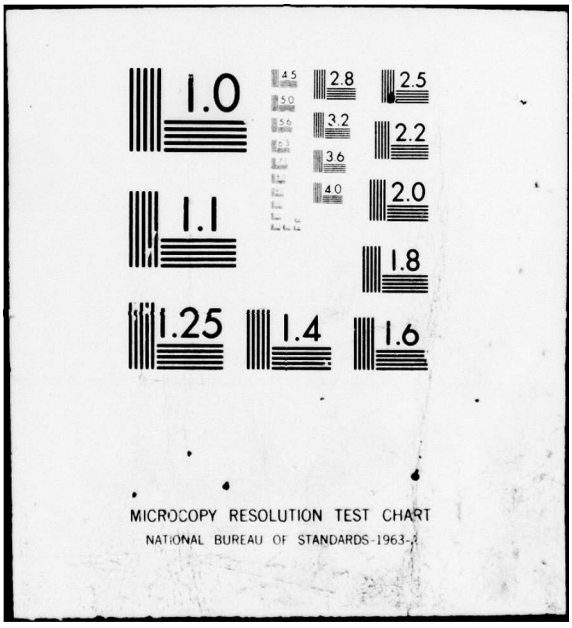
1.0
1.1
1.25
1.4
1.6
1.8
2.0
2.2
2.5
2.8
3.2
3.6
4.0
4.5
5.0
5.6
MICROCOPY RESOLUTION TEST CHART
NATIONAL BUREAU OF STANDARDS-1963-A

(12)

LEVEL II

RESEARCH AND DEVELOPMENT TECHNICAL REPORT

STRUCTURAL AND ELECTRICAL INVESTIGATION OF THE SILICON-SILICON DIOXIDE INTERFACE IN THERMALLY OXIDIZED SILICON

B. E. Deal
R. R. Razouk
FAIRCHILD CAMERA AND INSTRUMENT CORPORATION
Research and Development Laboratory
Palo Alto, CA 94304

October 1979

Final Report for Period 1 July 1978 – 30 June 1979

DISTRIBUTION STATEMENT

Approved for public release; distribution unlimited.

Prepared for:

US ARMY RESEARCH OFFICE
RESEARCH TRIANGLE PARK, NORTH CAROLINA 27709

REPORT DOCUMENTATION PAGE

READ INSTRUCTIONS BEFORE COMPLETING FORM

1. REPORT NUMBER: ECOM-78-0033-1	2. GOVT ACCESSION NO.
3. RECIPIENT'S CATALOG NUMBER	
4. TITLE (and Subtitle): STRUCTURAL AND ELECTRICAL INVESTIGATION OF THE SILICON-SILICON DIOXIDE INTERFACE IN THERMALLY OXIDIZED SILICON	5. TYPE OF REPORT & PERIOD COVERED: Final Report 1 July 1978-30 June 1979
	6. PERFORMING ORG. REPORT NUMBER
7. AUTHOR(s): B. E. Deal and R. R. Razouk	8. CONTRACT OR GRANT NUMBER(s): DAAG29-78-C-0033 Project No. 16245AEL
9. PERFORMING ORGANIZATION NAME AND ADDRESS: FAIRCHILD CAMERA AND INSTRUMENT CORPORATION, Research and Development Laboratory, 4001 Miranda Avenue, Palo Alto, CA 94304	10. PROGRAM ELEMENT, PROJECT, TASK AREA & WORK UNIT NUMBERS
11. CONTROLLING OFFICE NAME AND ADDRESS: U.S. Army Research Office, P.O. Box 12211, Research Triangle Park, NC 27709	12. REPORT DATE: October 1979 13. NUMBER OF PAGES: 47
14. MONITORING AGENCY NAME & ADDRESS(if different from Controlling Office)	15. SECURITY CLASS. (of this report): Unclassified 15a. DECLASSIFICATION/DOWNGRADING SCHEDULE: NA

16. DISTRIBUTION STATEMENT (of this Report)

Approved for public release, distribution unlimited.

17. DISTRIBUTION STATEMENT (of the abstract entered in Block 20, if different from Report)

18. SUPPLEMENTARY NOTES

The view, opinions, and/or findings contained in this report are those of the author(s) and should not be construed as an official Department of the Army position, policy, or decision, unless so designated by other documentation.

19. KEY WORDS (Continue on reverse side if necessary and identify by block number)

silicon oxidation, silicon dioxide, oxide charges, interface states

sub st

20. ABSTRACT (Continue on reverse side if necessary and identify by block number)

The dependence of fixed oxide charge density (Q_{ss}/q), interface state density (N_{st}), and electron spin resonance P_b signals on thermal oxidation process variables as well as their interrelationship has been investigated. Both n- and p-type silicon substrates having (111) and (100) orientation were employed in this study. Measurement techniques included conventional 1 MHz capacitance-voltage (C-V) analysis, quasistatic C-V analysis, and electron spin resonance. The oxide charges resulting from postoxidation in situ

anneal in nitrogen were found to be similar in nature and magnitude to those obtained following a similar treatment in argon. Some reduction in N_{st} was observed for thicker oxides following a post-metallization H_2 anneal. Strong evidence is obtained for a proportionality between ESR signals and interface states density with varying process parameters modifying the P_b to N_{st} relationship. The effects of iron ion implantation (before or after oxidation) on oxide charges and P_b signals has also been investigated. This work, in addition to clarifying the relationship between fixed oxide charges, interface states, and ESR P_b signals, demonstrates the significance of ESR as a tool in the characterization of the $Si-SiO_2$ system.

(6) STRUCTURAL AND ELECTRICAL INVESTIGATION OF THE $Si-SiO_2$ INTERFACE IN THERMALLY OXIDIZED SILICON

(9) RESEARCH AND DEVELOPMENT FINAL TECHNICAL REPORT

1 July 1978 — 30 June 1979

(15) CONTRACT NO. DAAG29-78-C-0033

DISTRIBUTION STATEMENT

Approved for public release; distribution unlimited.

(18) ARO, ECOM

(19) 16245.3-M-EL
78-0033-1

(11) Oct 79

(10) Prepared by

B. E. Deal and R. R. Razouk
Fairchild Camera and Instrument Corporation
Research and Development Laboratory
Palo Alto, California 94304

(12) 47

PURPOSE

The primary objective of this program was the investigation of the structural or defect nature, along with the electrical properties, of the $Si-SiO_2$ interface region of the thermally oxidized silicon system. The main thrust of the program was directed towards achieving a better understanding of the $Si-SiO_2$ interface through its dependence on process variables in order to provide semiconductor devices with better, more controlled parameters. To accomplish this objective, various analytical techniques for examining the electrical and structural properties of the $Si-SiO_2$ interface such as high and low frequency C-V measurements and electron spin resonance (ESR) were employed. A second objective was to investigate the effects of the incorporation of metallic impurities at the interface of thermally oxidized silicon since these impurities are known to adversely affect semiconductor device characteristics.

TABLE OF CONTENTS

LIST OF ILLUSTRATIONS

LIST OF TABLES

1.0 INTRODUCTION

A joint program was established between Fairchild Camera and Instrument Corporation and the United States Army Electronics Command, the purpose of which has been to obtain a better understanding of the $Si-SiO_2$ interface in thermally oxidized silicon and its dependence on process parameters. This understanding is critical to the production of integrated circuits with improved performance and reliability.

In the first year of the program, material and process parameters were selectively varied during the fabrication of MOS structures (1). These parameters included silicon substrate orientation and dopant type, dry O_2 oxidation temperature, and annealing/cooling conditions. Selected experiments using H_2O and O_2-HCl oxidizing ambients were also conducted. Characterization of the electrical charges associated with the thermally oxidized silicon system was carried out using conventional capacitance-voltage as well as quasistatic C-V measurements. Electron spin resonance techniques were employed by Ft. Monmouth personnel in order to investigate structural or defect properties of the $Si-SiO_2$ interface.

In the second year of the program, additional processing variables such as high-temperature in situ anneal ambients and their effect on oxide charges were examined. The effects of oxide thickness variations on the level of the charges measured as well as the ESR signals detected were also investigated. Other variables included dopant variations (type and concentration) and the incorporation of iron by ion implantation on the electrical and structural properties of the interface.

2.0 BACKGROUND

Thermally grown SiO_2 films play an important role in semiconductor device technology. These films which are produced by the oxidation of silicon are very stable chemically and have reproducible parameters under controlled oxidation conditions. The films are used both as temporary films for masking purposes and as permanent films for junction passivation, isolation of devices, or as actual integrated circuit components. Oxidation of the silicon substrates is carried out in a variety of ambients, typically dry O_2 or steam, at temperatures ranging from 900° to 1200°C. Extensive research has been carried out on the characterization of oxide charges (2-4) and the current understanding has been summarized by Deal (5). The following four types of charges are generally accepted:

(a) Fixed Oxide Charge (Q_{ss})

(b) Mobile Ionic Charge (Q_o)

(c) Interface State Charge (N_{st})

(d) Oxide Trapped Charge (N_{ot})

The exact origin of the fixed charge and the interface state charge is still in question and the work carried out in this program examines ESR signals reported in the $Si-SiO_2$ system, particularly P_b, with measured values of fixed oxide charge and interface state charge in order to determine any causal relationship between paramagnetic and electrical defects.

The dependence of the fixed oxide charge on process parameters such as oxidation temperature and postoxidation in situ annealing has been well characterized (6) and emphasis

in this program was placed on both interface state charges and ESR P_b signals.

Experiments completed in the first year demonstrated a relationship between the fixed oxide charge (Q_{ss}) and the interface state charge (N_{st}) of "as-oxidized" silicon samples. The dependence of the charges on material and process parameters (e.g., silicon type, silicon orientation, oxidation ambient, oxidation temperature, annealing and cooling conditions) has been established. Some interesting observations made on the diverse array of prepared samples are presented below:

(a) Oxide fixed charge as well as "as-oxidized" interface state charge densities were found to decrease with increasing temperature in the range of 800°-1200°C (7). Similar results were obtained with P_b signals (8) and previously observed ambiguities in their dependence on oxidation temperature (9,10) are thought to be a result of variations in the final cooling ambient.

(b) The silicon orientation effects commonly reported for both fixed charges and interface states have been observed and a ratio of approximately 3:1 established between (111) and (100) oriented silicon (both annealed and unannealed). Similarly, P_b signals were found to be higher for (111) than for (100) silicon oxides by a factor of approximately 3.

(c) A basic difference exists in interface state densities between samples pulled in an oxygen ambient, either fast or slow pull, and samples pulled in nitrogen. The latter seems to indicate the presence of both donor- and acceptor-like states, whereas oxygen-pulled

samples tend to indicate the absence of acceptor-like states.

(d) A relationship exists between fixed oxide charge density and interface state density of oxidized wafers which did not receive a low temperature hydrogen anneal. This relationship is found to be maintained in some cases after a hydrogen anneal step. This behavior tends to support the idea that Q_{ss} and N_{st} have some common origin, despite significant differences in detail.

(e) Interface state density levels were found to be lower in samples oxidized in steam (no H_2 postoxidation anneal), probably as a result of the hydrogen present in the oxidizing ambient. Reduced P_b values were also observed on these samples while interestingly no similar reduction in Q_{ss} has been noted.

(f) ESR signals detected on (111) silicon wafers seem to indicate a relationship between ESR signals and the interface state density of non-H_2-annealed samples. This relationship does not seem to be a direct one for all processing conditions, since nitrogen cooled samples showed a different N_{st} to ESR behavior than that obtained from oxygen-pulled samples.

(g) Reinducement of interface states by low temperature (500°C) annealing in nitrogen was observed by quasistatic C-V measurements and a corresponding increase in ESR signals added strength to a possible N_{st}-ESR relationship.

3.0 EXPERIMENTAL PROCEDURE

The silicon used for the electrical and oxide thickness measurements was obtained from Fairchild and was in the form of 2-inch diameter wafers, chem-mechanically polished on one side. Orientations were (100) and (111) and resistivity was 4-6 Ω-cm ($\sim 1\times10^{15}$ cm^{-3}), n-type phosphorus doped and 5-9 Ω-cm ($\sim 1\times10^{15}$ cm^{-3}), p-type, boron doped. Samples supplied to Ft. Monmouth for ESR measurements were in the form of 4×20 mm bars, laser or diamond scribed from 2-inch wafers obtained from Monsanto. These wafers were 200-500 μm thick and chem-mechanically polished on both sides; both n-type phosphorus and p-type boron doped wafers of resistivity $\geq$100 Ω-cm were used. Crystal growth was by the float zone process with a slice alignment of ±1° from (100) or (111) except for p-type (111) wafers which were 4° off (111) towards the (110) parallel to the flat.

The silicon samples were cleaned in sulfuric peroxide or hot sulfuric acid, aqua regia, 10:1 water:hydrofluoric acid, and isopropanol vapor, with appropriate deionized water rinses. They were then loaded into an oxidation furnace in the appropriate ambient and oxidized for a given time. Following oxidation the wafers were annealed in situ in nitrogen or argon and subsequently cooled in the anneal ambient (typical pull from the furnace was about 2 min). Where no anneal was required the wafers were pulled in the oxidizing ambient (typically 1-3 sec).

Dry oxygen was supplied from a liquid source, as were the nitrogen and hydrogen annealing gases. The water oxidation ambient was generated by the direct reaction of H_2 and O_2 in a pyrogenic system. Calibrated flowmeters were used to monitor and control gas mixtures in the proper ratios. The oxidation systems were conventional hot wall, resistance-heated furnaces with quartz tubes and high purity Mullite liners. Specially

designed boats and holders were used to support the silicon bars during the oxidation and cleaning processes.

After oxidation, aluminum dots approximately 1 μm thick and 750 μm in diameter were vacuum deposited at 25°C on the samples to be measured electrically. To avoid radiation effects, a nonelectron beam flash evaporation system was employed. Oxide thicknesses were determined using a Rudolph Model 436-200E ellipsometer, and ranged from approximately 50 Å to 2000 Å.

One half of each wafer was annealed in a 25% H_2 in N_2 mixture for 10 minutes at 450°C. These H_2-annealed samples were used for measurement of Q_{ss}, the oxide fixed charge. Conventional C-V analysis equipment was used for this measurement.

Values of N_{st}, the interface state density, were determined by the quasistatic C-V technique (11,12). This method is based on the proportionality that exists between the incremental MOS capacitance and the charging current in the structure when it is subjected to a linear voltage ramp. As a result of this proportionality a low-frequency thermal equilibrium MOS capacitance-voltage curve can be obtained. The quasistatic and high frequency curves are then used to extract the interface state density distribution in the bandgap. This method is valid in the interval of the forbidden gap extending from the inversion threshold to a position about 200 mV from the majority carrier band edge. The relationship between the silicon surface potential and the applied voltage is obtained by the integration of the quasistatic C-V curve as proposed by Berglund (13).

A schematic diagram of the automated capacitance-voltage analysis system is shown in Fig. 3-1 and shows the most recent

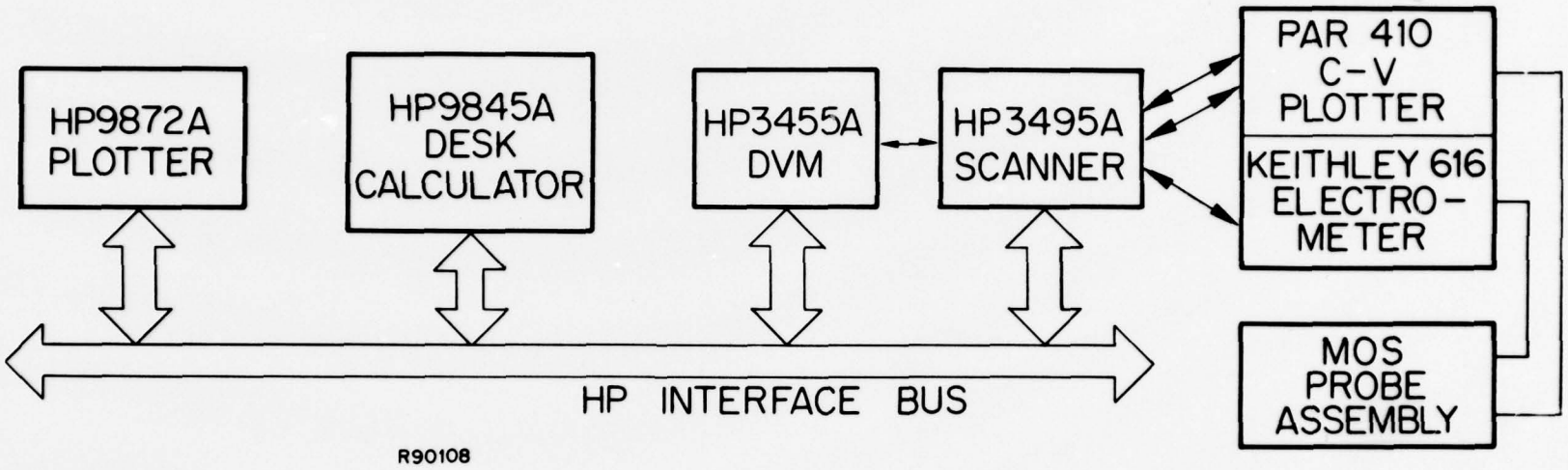

Fig. 3-1. Schematic diagram of the computerized quasistatic C-V analysis system.

updates in the system which include a more advanced desktop calculator and plotter. Automated measurements of the ramp voltage in conjunction with either the capacitance or the charging current in the MOS structure are used to generate the high frequency and quasistatic C-V curves, respectively. Accuracy of the quasistatic method in determining interface states is estimated to be $10^{10}/cm^2$-eV at midgap.

Measurements of interface state density will be reported either in terms of midgap N_{st} values or by showing the entire interface state density distribution. Midgap values will be used primarily when they are indicative of the major trends related to process variations. The reported Q_{ss}/q and N_{st} values represent an average over several capacitors on each wafer and should be regarded as such. Variations approaching 20% have been observed on a single wafer and this should be taken into account when drawing conclusions dealing with the effects of process parameters on Q_{ss}/q and N_{st}.

4.0 RESULTS AND DISCUSSION

4.1 High Temperature Annealing in Nitrogen and Argon

The annealing of thermally grown silicon dioxide films in inert ambients, particularly nitrogen, has been used extensively in integrated circuit fabrication. Often the anneal is carried out in situ at the oxidizing temperature. The effects of this anneal on fixed oxide charges are known to be a reduction in charge densities, particularly for anneals around 1000°C and for oxide thicknesses greater than 1000 Å. Differences have however been reported between annealing in nitrogen and in argon with respect to the resulting oxide charges (14) and a reaction between nitrogen and the silicon substrate has been proposed (15,16). In the experiments reported here, n- and p-type wafers, (100) and (111), 4-6 Ω-cm, and 4×20 mm bars of resistivity greater than 100 Ω-cm were used. The wafers were oxidized at 1000° or 1200°C for 360 or 60 min, respectively, and subsequently annealed in situ in nitrogen or argon for 10 or 60 min at the oxidizing temperature.

Typical interface state density energy distributions (N_{st}) for both nitrogen and argon are shown in Fig. 4-1 for n-type (100) samples oxidized and annealed at 1200°C and indicate a basic similarity in both magnitude and energy distribution for wafers annealed in either gas. Characteristic of the measurements are a peak of interface states above midgap (0.2-0.3 eV below the conduction band), a minimum around midgap, and a high level of interface states (probably a peak) below midgap. Similar results were obtained on p-type (100) samples (17) showing a definite peak below midgap of smaller magnitude than for n-type wafers. N_{st} values obtained from quasistatic measurements on p-type wafers were found to be generally lower than values obtained on n-type wafers in agreement with previous observations (1).

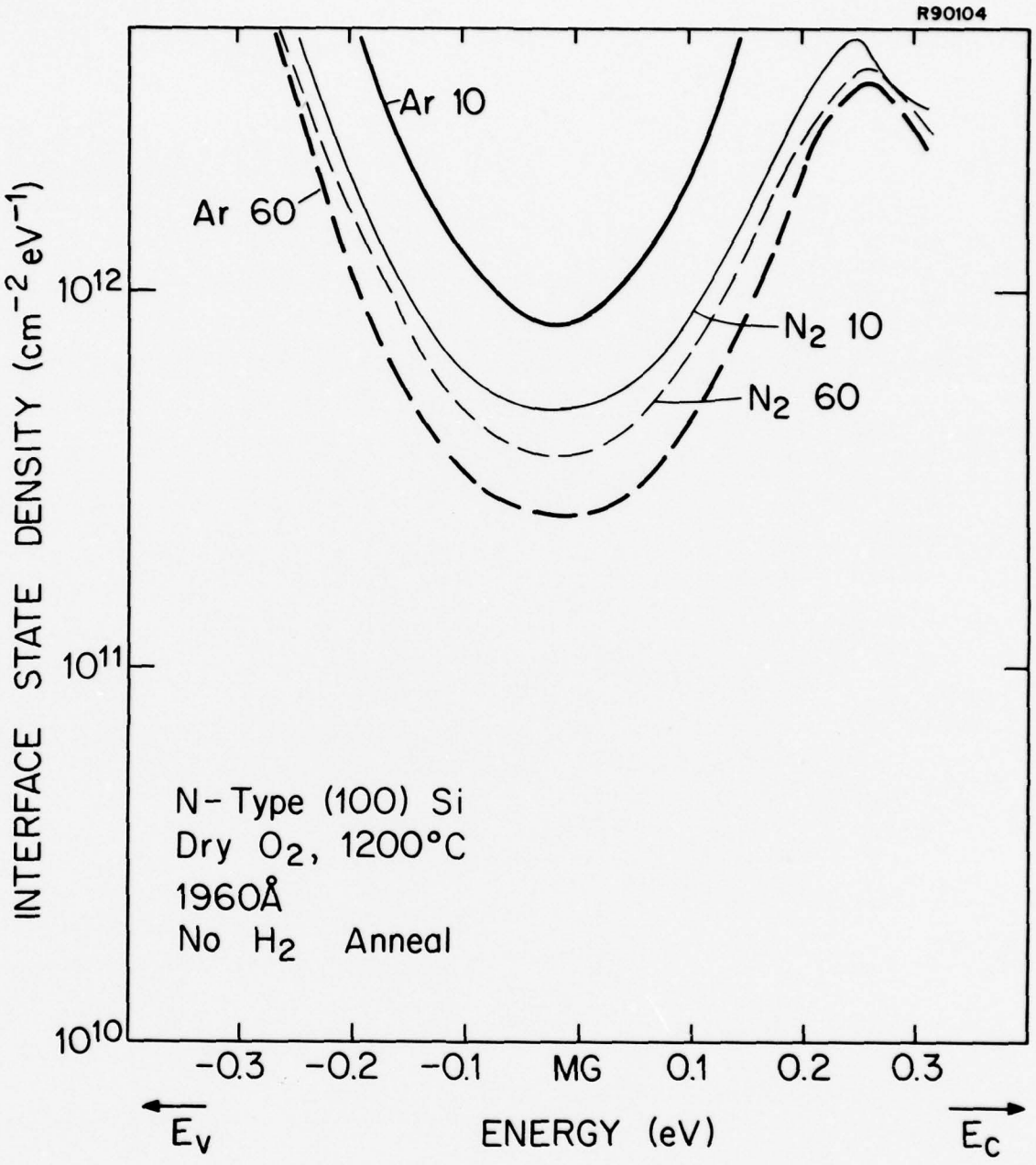

Fig. 4-1. Interface state density distribution for n-type (100) silicon oxidized in dry O_2 at 1200°C and annealed in situ for 10 or 60 minutes in nitrogen or argon. Samples did not receive a low temperature hydrogen anneal.

Other results indicate a higher level of interface states in argon annealed samples for short anneal time (10 min) and a lower level for longer anneal time (60 min) when compared to nitrogen annealed samples for 10 and 60 min, respectively. Prolonged anneal times in either gas seemed to reduce "as-oxidized" interface states at 1000°C and 1200°C while increasing fixed oxide charge density at 1200°C.

ESR results obtained at Ft. Monmouth by measuring non-H_2-annealed samples and a discussion of the relation between P_b signals and N_{st} values at midgap are presented in Section 4.5.

4.2 Oxide Thickness Variations

The effects of oxide thickness on oxide fixed charge (Q_{ss}/q), interface states (N_{st}), and electron spin resonance (ESR) were investigated. The samples used in the investigation were n-type (100) and (111) wafers, 4-6 Ω-cm, and 4×20 mm, $\geq$100 Ω-cm bars, which were oxidized in dry O_2 at 1000°C for times ranging from 2 min to 6 hours. The resulting oxide thicknesses ranged from 50 Å to 2010 Å. Following oxidation the wafers were pulled from the oxidizing ambient in less than 3 sec (fast pull).

Due to the effects the metal-semiconductor work function has on oxide fixed charge measurements, and the uncertainty in the value of ϕ_{ms}, a plot of flatband voltage (V_{FB}) versus oxide thickness (x_o) was prepared (17). Analysis of the plot showed that a straight line could be used to fit all the data, which indicates a constant fixed oxide charge. Values of Q_{ss}/q obtained were $0.68\times10^{11}/cm^2$ and $3.3\times10^{11}/cm^2$ for (100) and (111) substrates, respectively. N_{st} values at midgap ranged from 5 to $11\times10^{11}/cm^2$-eV for (100) and from 18 to $27\times10^{11}/cm^2$-eV for (111) with no particular trends observable. Following low-

temperature hydrogen anneal, higher N_{st} values were measured for thinner oxides as shown by a plot of interface state density (N_{st}) at midgap versus inverse oxide thickness ($1/x_o$) in Fig. 4-2. Since there is no evidence of N_{st} dependence on oxide thickness prior to H_2 anneal, oxide growth rate differences are unlikely to be responsible for the observed dependence following H_2 anneal. The hydrogen anneal mechanism is postulated to occur as a result of several simultaneous reactions such as the interaction between water and aluminum to generate active hydrogen according to the reaction

$$2\ Al + 3\ H_2O \underset{k_{-1}}{\overset{k_1}{\rightleftharpoons}} Al_2O_3 + 6\ (H\cdot), \qquad [1]$$

the dissociation of molecular hydrogen

$$H_2 \underset{k_{-2}}{\overset{k_2}{\rightleftharpoons}} 2\ (H\cdot), \qquad [2]$$

and the complexing of silicon surface bonds by the active hydrogen

$$H\cdot + - \underset{|}{\overset{|}{Si}} - \underset{k_{-3}}{\overset{k_3}{\rightleftharpoons}} - \underset{|}{\overset{|}{SiH}}. \qquad [3]$$

All the above reactions are thought to occur simultaneously and an oxide thickness dependence such that thinner oxides have higher interface state density can result from a smaller amount of active hydrogen being retained in the thinner oxides. The active hydrogen formed either through reaction [1], [2], or both with rate constants k_1 and k_2 would in the case of thinner oxides be more likely to escape to the ambient and form molecular hydrogen through reaction [2] with rate constant [k-2].

Another point of interest evident from Fig. 4-2 is the relationship between the interface state density measured on

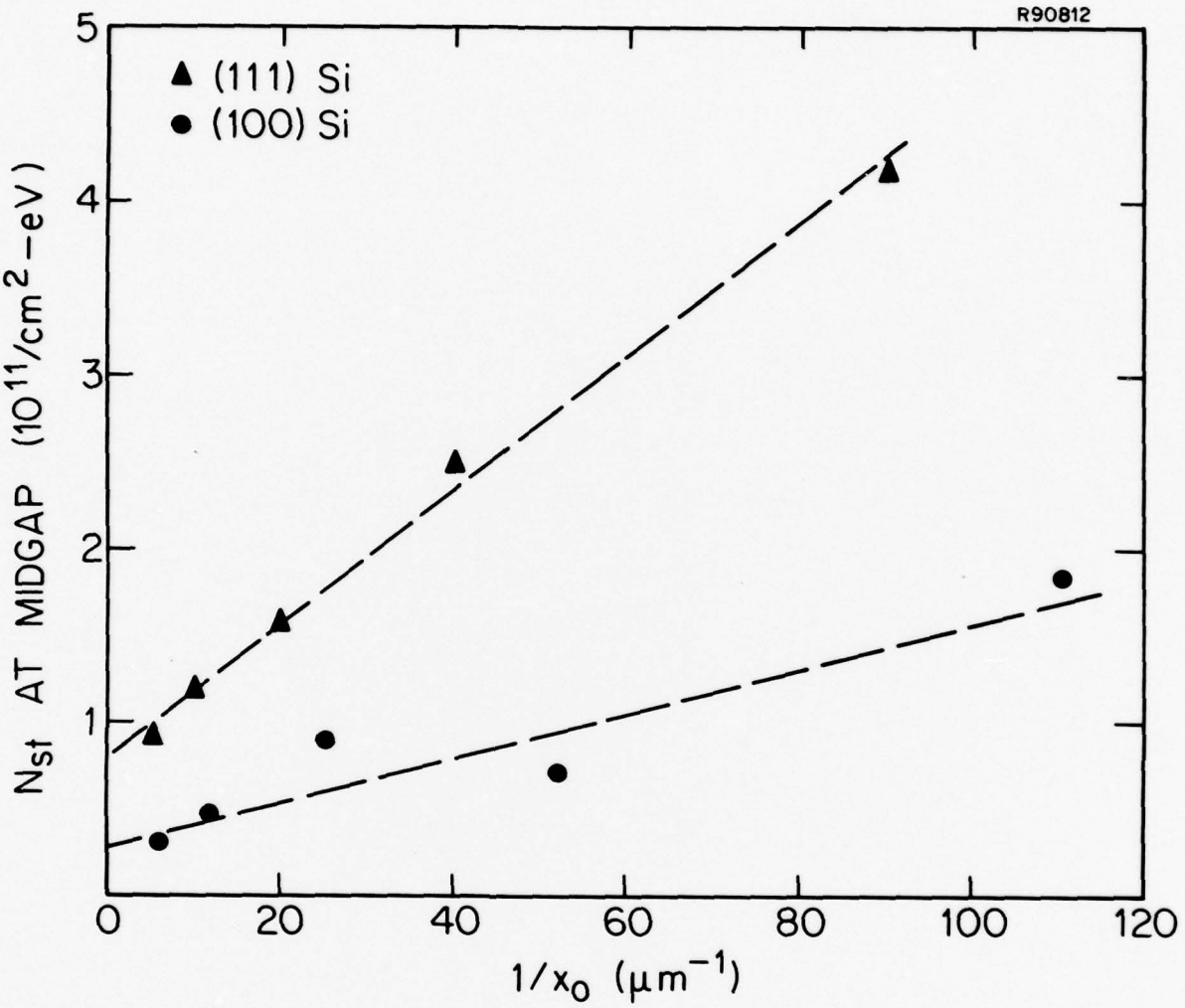

Fig. 4-2. Interface state density (N_{st}) at midgap versus inverse oxide thickness for (100) and (111) silicon samples oxidized in dry O_2 at 1000°C (O_2FP) and given a post-metallization H_2 anneal at 450°C for 10 min in a 25% H_2 in N_2 ambient.

(100) and that measured on (111). The line through the (100) points was arrived at by taking into account a 3:1 ratio for (111):(100). This is further evidence of a strong relationship between Q_{ss} and N_{st} since this ratio is well known for Q_{ss}. Furthermore, the observation of a changing interface state density accompanied by a constant Q_{ss} does not contradict the basic Q_{ss}-N_{st} relationship, since appropriate annealing treatments should be able to discriminate between any detailed chemical differences of Q_{ss} and N_{st}. Changes in ESR signals due to these H_2 annealings although not measurable at this time would undoubtedly be of great interest.

4.3 Dopant Concentration Variations

The investigation of the effects of variations in dopant type and concentration on ESR signals and oxide charges were carried out by using p- and n-type (111) wafers of resistivity 25, 50, and 100 Ω-cm. The wafers were oxidized at 1000°C for 360 minutes in dry O_2 and cooled in either nitrogen or oxygen. The significance of this experiment derives from the fact that oxide charges and ESR signals throughout this program have been measured on silicon material of differing resistivities, with 4-9 Ω-cm silicon used for oxide charge measurements, and 100 Ω-cm silicon used for ESR measurements. This was done to operate in the region most suitable for each measurement technique. Effects due to dopants, particularly as they relate to ESR measurements, are therefore necessary to get a complete picture of the process dependence of both Q_{ss}, N_{st}, and ESR and their relationship to each other.

Information about the various runs carried out under this section of the program are tabulated in Table 4-1. Run numbers, resistivity, processing steps, oxide thickness, and oxide charges are included. No observable dopant concentration

Table 4-1

Values of Fixed Oxide Charge (Q_{ss}) and Interface State Density (N_{st}) for n- and p-type (111) Silicon Samples of Various Resistivities Oxidized at 1000°C in Dry Oxygen

Run No.	Silicon Type Orient.	Resistivity (Ω-cm)	Ox/ Anneal Ambient	Ox/ Anneal Time* (min)	Cool Condition**	Thickness (μm)	Q_{ss}/q ($10^{11}/cm^2$)	Midgap N_{st} ($10^{11}/cm^2$-eV)	
								No Anneal	H_2 Anneal
FM-71	n-(111)	25	O_2/-	360/0/0	O_2 FP	0.200	4.18	30	0.81
FM-72	"	"	O_2/N_2	360/10/2	N_2 SP	"	2.10	18	0.30
FM-73	"	50	O_2/-	360/0/0	O_2 FP	0.199	4.32	29	0.79
FM-74	"	"	O_2/N_2	360/10/2	N_2 SP	"	2.11	21	0.31
FM-75	"	100	O_2/-	360/0/0	O_2 FP	0.202	3.68	37	0.93
FM-76	"	"	O_2/N_2	360/10/2	N_2 SP	"	2.08	23	0.37
FM-77	p-(111)	25	O_2/-	360/0/0	O_2 FP	0.200	4.24	31	0.98
FM-78	"	"	O_2/N_2	360/10/2	N_2 SP	0.201	2.30	15	0.45
FM-79	"	50	O_2/-	360/0/0	O_2 FP	0.203	4.16	29	1.1
FM-80	"	"	O_2/N_2	360/10/2	N_2 SP	"	2.36	18	0.55
FM-81	"	100	O_2/-	360/0/0	O_2 FP	0.203	4.26	35	1.57
FM-82	"	"	O_2/N_2	360/10/2	N_2 SP	"	2.31	21	0.67

*Oxidation time/anneal time in N_2/pull time.

**SP = slow pull (2 min), closed elephant.
FP = fast pull (<3 sec), closed elephant.

effects were noted on oxide charges in this doping range. Values of fixed oxide charge density (Q_{ss}/q) for both n- and p-type (111) silicon were 4.24 ± 0.23 ($10^{11}/cm^2$) for oxygen-pulled wafers and 2.9 ± 0.14 ($10^{11}/cm^2$) for nitrogen-pulled wafers.

Interface state density at midgap following hydrogen anneal was different for n- and p-type wafers with average values of 0.87 ± 0.2 ($10^{11}/cm^2$-eV) and 1.24 ± 0.3 ($10^{11}cm^2$-eV) for n- and p-type silicon, respectively, for oxygen-pulled wafers, and 0.3 ± 0.05 ($10^{11}/cm^2$-eV) and 0.55 ± 0.1 ($10^{11}/cm^2$-eV) for nitrogen-pulled wafers.

ESR signals measured at Ft. Monmouth also indicated no dopant concentration effects although some difference was noted due to dopant type. ESR results and comparison with N_{st} and Q_{ss}/q data will be discussed in Section 4.5.

4.4 Incorporation of Metallic Impurities

Experiments were carried out to investigate the effects of the incorporation of metallics at the Si-SiO_2 interface on oxide charges as well as ESR signals. Iron ion implantation was employed for that purpose. N-type wafers, (100) and (111), with resistivity of 4-6 Ω-cm were used for oxide charge measurements, while 100 Ω-cm, 4×20 mm bars, were used in ESR measurements. The incorporation of iron was carried out by ion implantation either in bare silicon to a depth of 450 Å or in oxidized silicon wafers (1000 Å SiO_2) at the interface. The dose employed was $10^{13} \pm 10\%$ (cm^{-2}). Following implantation the bare silicon wafers were oxidized to a final oxidation thickness of 1000 Å. All oxidations were carried out in a dry O_2 ambient at 1000°C for 120 min, followed by a 10 min anneal and a slow pull (2 min) in nitrogen. The effects of high temperature annealing were investigated by means of a 60 min

anneal at 1000°C in a 10% hydrogen in nitrogen ambient for selected samples.

A summary of the various process conditions used for these series of experiments is included in Table 4-2 (Run No. FMF-13A through FMF-28B). Fixed oxide charge measurements (Q_{ss}/q), interface state density measurements (N_{st}), and mobile ionic charge measurements (Q_o/q) are also included. The data in Table 4-2 should be examined without losing sight of the following factors.

(a) Samples FMF-13B through FMF-28B received no hydrogen anneal treatments and therefore can only be characterized with an "effective" Q_{ss}/q which contains contributions from interface states.

(b) Interface state densities are substantial for damaged wafers which receive no anneal, typically higher than $1\times10^{13}/cm^2$-eV and outside the measurement capability of the quasistatic technique.

(c) Large values were obtained for Q_o/q probably as a result of the high temperature anneal in a hydrogen/nitrogen ambient. No Q_o/q values are measurable on non-H_2-annealed wafers since a reduction of interface states occurs during heat cycling making the measurement ambiguous. Furthermore, the presence of mobile ionic charges can result in higher measured densities for both oxide fixed charge and interface states.

The major findings from this part of the program are:

(a) For silicon wafers oxidized both prior to and following iron ion implantation, no interface state density

Table 4-2

Process Variations and Measured Oxide Charges for Experiments Dealing with the Incorporation of Metallic Impurities at the Si-SiO_2 Interface

Run No.	Orient.	Ox.[a]	Iron[b] Ion Impl. Depth (Å)	Ox.[a]	High[c] Temp. Anneal	Q_{ss}/q[d] ($10^{11}/cm^2$)	Midgap N_{st} ($10^{11}/cm^2$-eV)	Q_o/q[e] ($10^{11}/cm^2$)
FM-13A	(100)	-	450	✓	✓	4.3	0.27	3.2
FM-13B	(100)	-	450	✓	-	NA	2.33	NA
FMF-14A	(100)	-	-	✓	✓	2.45	1.13	2.1
FMF-14B	(100)	-	-	✓	-	NA	>50	NA
FMF-17A	(111)	-	450	✓	✓	9	1.4	8.9
FMF-17B	(111)	-	450	✓	-	NA	11.3	NA
FMF-18A	(111)	-	-	✓	✓	4.5	1.1	4.0
FMF-18B	(111)	-	-	✓	-	NA	>50	NA
FMF-21A	(100)	✓	1,000	-	✓	4.2	0.42	4.3
FMF-21B	(100)	✓	1,000	-	-	NA	>50	NA
FMF-22A	(100)	✓	-	-	✓	3.1	2.4	2.7
FMF-22B	(100)	✓	-	-	-	NA	>50	NA
FMF-27A	(111)	✓	1,000	-	✓	5.67	1.0	6.4
FMF-27B	(111)	✓	1,000	-	-	NA	>50	NA
FMF-28A	(111)	✓	-	-	✓	6.3	4.7	5.0
FMF-28B	(111)	✓	-	-	-	NA	>50	NA

[a] Dry O_2, 1000°C, 120 min, nitrogen slow pull.

[b] Dose $10^{13} \pm 10\%$ (cm^{-2}).

[c] 10% hydrogen in nitrogen, 1000°C, 60 min.

[d] Q_{ss}/q values are applicable only when Q_o/q and N_{st} make minimum contributions to flatband voltage.

[e] At 300°C--50 V/μm (+ bias)
--30 V/μm (- bias)
Heat cycling results in the anneal of interface states in non-H_2-annealed samples making the determination of Q_o/q ambiguous.

peaks were observed in the portion of the bandgap where the measurement is valid.

(b) The level of interface states was typically lower for iron implanted interfaces. This was evident in wafers which received the 1000°C anneal (10% H_2 in N_2) as well as those which were not annealed. It is felt however that this result is ambiguous due to the presence of a substantial number of mobile ions, some of which may be gettered by the iron, and some of which contribute to erroneous fixed oxide charge and interface state density measurements.

(c) Measurements carried out at Ft. Monmouth are summarized in Table 4.3. Four ESR species can be observed: P_b; P_c (18) in the silicon bulk due to neutral iron (19); and damage sites in both silicon bulk and oxide, such as occur with neon and oxygen (20). The damage signals disappear after annealing, as expected. The implanted iron does not seem to have a remarkable effect on P_b, although the signal from FMF-9B is unusually strong. P_c is not decisively affected by the implanted Fe, which is surprising in view of the large interface concentration. Since both implanted and inherent bulk Fe must be reduced to Fe^o for ESR visibility, different annealing efficiencies in the two regions may be the explanation.

(d) Most wafers which received an H_2 anneal following implantation showed low interface state densities at midgap ($<5\times10^{11}/cm^2$-eV) and no measurable ESR signal. Samples with no H_2 anneal had high interface states ($>50\times10^{11}/cm^2$-eV) except sample FMF-13B with $11.3\times10^{11}/cm^2$-eV and a corresponding ESR signal of

Table 4-3

Electron Spin Resonance and Oxide Charge Densities for Samples with Iron Implants at the $Si-SiO_2$ Interface

Run Number		Process Sequence	ESR Interf. Signal	Impl. Signal in Si	Impl. Signal in Ox	Iron Signal in Si	Q_{ss}/q	Q_o/q	Midgap N_{st}
(100 Ω-cm)	(4-6 Ω-cm)		(10^{11} spins/cm^2)				(10^{11}/cm^2)	(10^{11}/cm^2)	(10^{11}/cm^2-eV)
FMF-1A	None	Im	6	-	-	0	-	-	-
FMF-1B	"	Im/An*	4.5	156	-	0	-	-	-
FMF-2A	None	None	9	-	-	0	-	-	-
FMF-2B	"	An*	8	42	-	0	-	-	-
FMF-3A	None	Im/An**	2	-	-	0	-	-	-
FMF-3B	"	Im/An†	6.5	10	-	160	-	-	-
FMF-4A	None	An**	-	-	-	130	-	-	-
FMF-4B	"	An†	-	-	-	110	-	-	-
FMF-7A	FMF-17A	Im/Ox/An†	-	-	-	90	9	8.9	1.4
FMF-7B	FMF-17B	Im/Ox	7	-	-	80	NA	NA	11.3
FMF-8A	FMF-18A	Ox/An†	-	-	-	55	4.5	4.0	1.1
FMF-8B	FMF-18B	Ox	13	-	-	0	NA	NA	>50
FMF-9A	FMF-27A	Ox/Im/An†	-	-	-	110	5.67	6.4	1.0
FMF-9B	FMF-27B	Ox/Im	22	60	180	0	NA	NA	>50
FMF-10A	FMF-28A	Ox/An†	-	-	-	90	6.3	5	4.7
FMF-10B	FMF-28B	Ox	11	-	-	0	NA	NA	>50

Im = Implant; Ox = Oxidation; An = Anneal.

*Anneal at 600°C, 60 min, N_2.

**Anneal at 1000°C, 60 min, N_2.

†Anneal at 1000°C, 60 min, 10% H_2 in N_2.

7×10^{11} spins/cm^2 maintaining the usual correspondence between P_b and N_{st}.

4.5 Relationship Between ESR Signals and N_{st} Densities

The evaluation of electron spin resonance (ESR) techniques as a tool in the study of defect centers at the Si-SiO_2 interface (18,19,21) is one of the main objectives of this program. Three paramagnetic defect species designated P_a, P_b, and P_c are commonly associated with thermally oxidized silicon. In this investigation, the P_b center, its dependence on process parameters, and its correlation with oxide charges at the Si-SiO_2 interface have been examined. Although inconsistent evidence of P_b-Q_{ss} correlation has been observed (9), any such correlation appears to be limited to cases where N_{st} and Q_{ss} are also correlated. We have therefore concentrated on exploring the relationship between P_b and N_{st}.

During the first year of the program, the data indicated a relationship between the interface state density in non-H_2-annealed samples and ESR signals. Both P_b and N_{st} were found to be greatly reduced by steam oxidations and hydrogen annealing (22). Both P_b and N_{st} were also regenerated by extended N_2 anneals at 500°C. Nevertheless, various processing effects modify the relationship between P_b and N_{st}, and a summary of these is presented below.

Tables 4-4 through 4-7 summarize some of the more relevant information on oxide charges and ESR measurements. Results are tabulated according to process variations in such a manner that all data for samples oxidized and cooled in O_2 (O_2FP) are presented in one table, data for wafers oxidized in O_2 and annealed/cooled in argon in another table, etc. This tabulation system was chosen to clarify some of the observed N_{st} versus ESR relationships.

Table 4-4

Values of Fixed Oxide Charge (Q_{ss}), Interface State Density (N_{st}), and Electron Spin Resonance (P_b) for n- and p-Type Silicon Wafers Oxidized and Cooled in Dry Oxygen

Run No.	Silicon Type Orient.	Oxidation Temp. (°C)	Ox./Anneal Time* (min)	Oxide Thick. (μm)	Q_{ss}/q ($10^{11}/cm^2$)	Midgap N_{st} ($10^{11}/cm^2$-eV)	ESR P_b (10^{11} spins/cm^2)
						No H_2 Anneal	
FM-14	n-(100)	800	4800/0/0	0.119	1.88	10	6.4
"	n-(111)	"	"	0.180	5.0	34	18
FM-11	n-(100)	1000	400/0/0	0.185	0.87	8	2
"	n-(111)	"	"	0.22	3.35	16	4
FM-32	p-(100)	"	400/0/0	0.183	1.2	2.5	0.6
"	p-(111)	"	"	0.215	3.9	12	8.5
FM-61	n-(100)	"	4/0/0	0.009	0.68	11	4.8
"	n-(111)	"	"	0.011	3.3	21	17
FM-62	n-(100)	"	13/0/0	0.019	0.68	8.7	7.2
"	n-(111)	"	"	0.025	3.3	25	27
FM-63	n-(100)	"	40/0/0	0.039	0.68	8	5.2
"	n-(111)	"	"	0.051	3.3	22.5	20
FM-64	n-(100)	"	120/0/0	0.083	0.68	5	0.8
"	n-(111)	"	"	0.102	3.3	18	20
FM-65	n-(100)	"	360/0/0	0.171	0.68	8.5	2.8
"	n-(111)	"	"	0.201	3.3	17	26
FM-17	n-(100)	1200	60/0/0	0.194	<0.10	2.5	1.2
"	n-(111)	"	"	0.194	2.33	12	1.5
FM-29	p-(100)	"	"	0.196	0.28	0.9	0
"	p-(111)	"	"	"	1.92	6.5	0

*Oxidation time/anneal time in N_2 or Ar/pull time.

Table 4-5

Values of Fixed Oxide Charge (Q_{ss}), Interface State Density (N_{st}), and Electron Spin Resonance (P_b) for n-Type Silicon Wafers Oxidized in Dry Oxygen and Annealed in Nitrogen

Run No.	Silicon Orient.	Oxidation Temp. (°C)	Ox./ Anneal Time*(min)	Oxide Thick. (μm)	Q_{ss}/q (10^{11}/cm^2)	Midgap N_{st} (10^{11}/cm^2-eV)	ESR P_b (10^{11} spins/cm^2)
						No H_2 Anneal	
FM-16	(100)	800	4800/10/2	0.116	1.58	20	11.2
"	(111)	"	"	0.176	3.59	27	17
FM-13	(100)	1000	400/10/2	0.185	<0.10	11	6.8
"	(111)	"	"	0.22	1.32	≥50	15
FM-51	(100)	"	360/10/2	0.172	0.24	12	5.6
"	(111)	"	"	0.203	1.93	25	11
FM-52	(100)	"	360/60/2	0.172	0.21	8	5.6
"	(111)	"	"	0.202	1.41	20	15
FM-19	(100)	1200	60/10/2	0.196	<0.10	6	2
"	(111)	"	"	0.196	2.43	23	17
FM-45	(100)	"	60/10/2	0.196	0.22	4.5	3.6
"	(111)	"	"	0.198	2.04	22	15
FM-46	(100)	"	60/60/2	0.196	0.65	3.7	2.4
"	(111)	"	"	0.198	2.47	10	11

*Oxidation time/anneal time in N_2 or Ar/pull time.

Table 4-6

Values of Fixed Oxide Charge (Q_{ss}), Interface State Density (N_{st}), and Electron Spin Resonance (P_b) for p-Type Silicon Wafers Oxidized in Dry Oxygen and Annealed in Nitrogen

Run No.	Silicon Orient.	Oxidation Temp. (°C)	Ox./ Anneal Time* (min)	Oxide Thick. (μm)	Q_{ss}/q ($10^{11}/cm^2$)	Midgap N_{st} ($10^{11}/cm^2$-eV)	ESR P_b (10^{11} spins/cm^2)
						No N_2 Anneal	
FM-34	(100)	1000	400/10/2	0.183	0.26	4	9.6
"	(111)	"	"	0.215	1.94	14	19
FM-53	(100)	"	360/10/2	0.172	0.57	14	3.2
"	(111)	"	"	0.203	2.84	17	13
FM-54	(100)	"	360/60/2	0.172	0.52	8	2.8
"	(111)	"	"	0.203	1.99	13	13
FM-31	(100)	1200	60/10/2	0.196	<0.10	4	4.8
"	(111)	"	"	0.196	2.30	13	14
FM-43	(100)	"	60/10/2	0.196	0.11	3.5	0
"	(111)	"	"	0.198	1.94	11.5	12
FM-44	(100)	"	60/60/2	0.196	0.43	1.7	4.4
"	(111)	"	"	0.196	2.49	9	8

*Oxidation time/anneal time in N_2 or Ar/pull time.

Table 4-7

Values of Fixed Oxide Charge (Q_{ss}), Interface State Density (N_{st}), and Electron Spin Resonance (P_b) for n- and p-Type Silicon Wafers Oxidized in Dry Oxygen and Annealed in Argon

Run No.	Silicon Orient.	Oxidation Temp. (°C)	Ox./Anneal Time* (min)	Oxide Thick. (μm)	Q_{ss}/q (10^{11}/cm^2)	Midgap N_{st} (10^{11}/cm^2-eV) No H_2 Anneal	ESR P_b (10^{11} spins/cm^2) No H_2 Anneal
FM-55	n-(100)	1000	360/10/2	0.172	0.25	13	6
"	n-(111)	"	"	0.203	2.25	30	12
FM-56	n-(100)	"	360/60/2	0.172	0.27	10	6.4
"	n-(111)	"	"	0.203	"	25	10
FM-57	p-(100)	"	360/10/2	0.169	0.56	12	4.4
"	p-(111)	"	"	0.203	2.77	18	13
FM-58	p-(100)	"	360/60/2	0.171	0.171	11	3.4
"	p-(111)	"	"	0.203	1.93	20	1.2
FM-47	n-(100)	1200	60/10/2	0.196	0.11	8	3.2
"	n-(111)	"	"	"	2.28	25	10
FM-48	n-(100)	"	60/60/2	"	0.22	2.5	2.8
"	n-(111)	"	"	"	2.28	25	12
FM-49	p-(100)	"	60/10/2	"	<0.10	2.5	3.6
"	p-(111)	"	"	"	1.73	20	11
FM-50	p-(100)	"	60/60/2	0.195	<0.10	1.5	2.8
"	p-(111)	"	"	0.196	1.73	25	12

*Oxidation time/anneal time in N_2 or Ar/pull time.

Process variations such as annealing and cooling were observed to play a substantial role in oxide charges and ESR signals. It was also noted that these variations affected the relationship between ESR and N_{st}. Figure 4-3 illustrates the relationship for samples oxidized in dry O_2 at various temperatures and cooled in O_2 (O_2FP). Both (100) and (111) samples, n- and p-type, are shown and although scatter is evident in the data, a clear correlation seems to exist between the ESR data and the midgap values of N_{st} as measured by the quasistatic technique.

In presenting the data for samples oxidized in dry O_2 and annealed/cooled in nitrogen, we have separate plots, Figs. 4-4 and 4-5, for n- and p-type samples, respectively. It is noteworthy that Fig. 4-4 could mostly follow the same line as Fig. 4-3, while Fig. 4-5 shows quite a different behavior. The cause of this difference between n- and p-type behavior is not clear at this time, although typically some difference has been noted between the two types, the n-type wafers yielding higher interface state density values. The results for argon annealed/cooled wafers are given in Fig. 4-6.

There are other considerations which make it difficult to establish a broad and conclusive relationship between P_b and N_{st} for diverse physical and chemical situations. A different type of interface states (donor- or acceptor-like) seem to arise from different processing conditions (1). Nitrogen and argon anneal/cool seem to result in the creation of both types of states, whereas oxygen-cooled samples (O_2FP) seem to be characterized by predominantly donor states in the lower portion of the bandgap. How the nature of the states affects the ESR signals is not clear. Furthermore, values of N_{st} reported here are at midgap with some potential applied to the interface while ESR values are measured in a "no-bias"

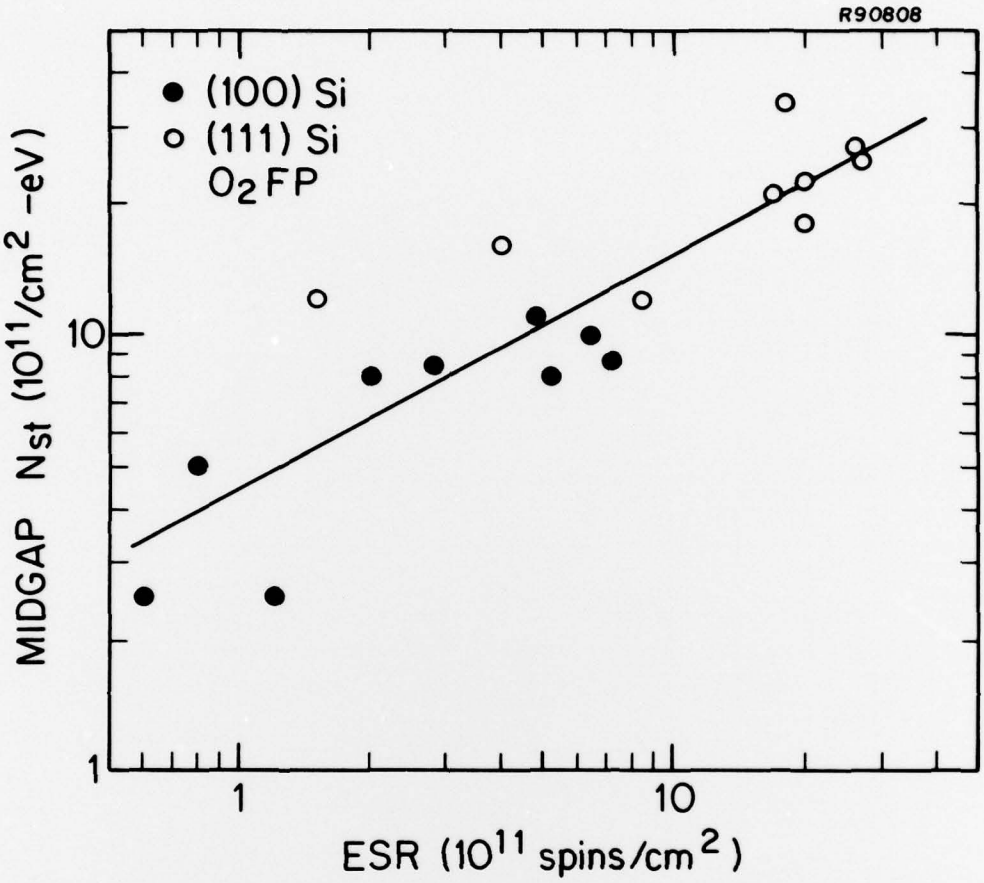

Fig. 4-3. Midgap interface state density (N_{st}) versus electron spin resonance (P_b) signals for n- and p-type (100) and (111) wafers oxidized in dry O_2 at 800°, 1000°, and 1200°C and cooled in dry O_2. Wafers received no postoxidation hydrogen anneal.

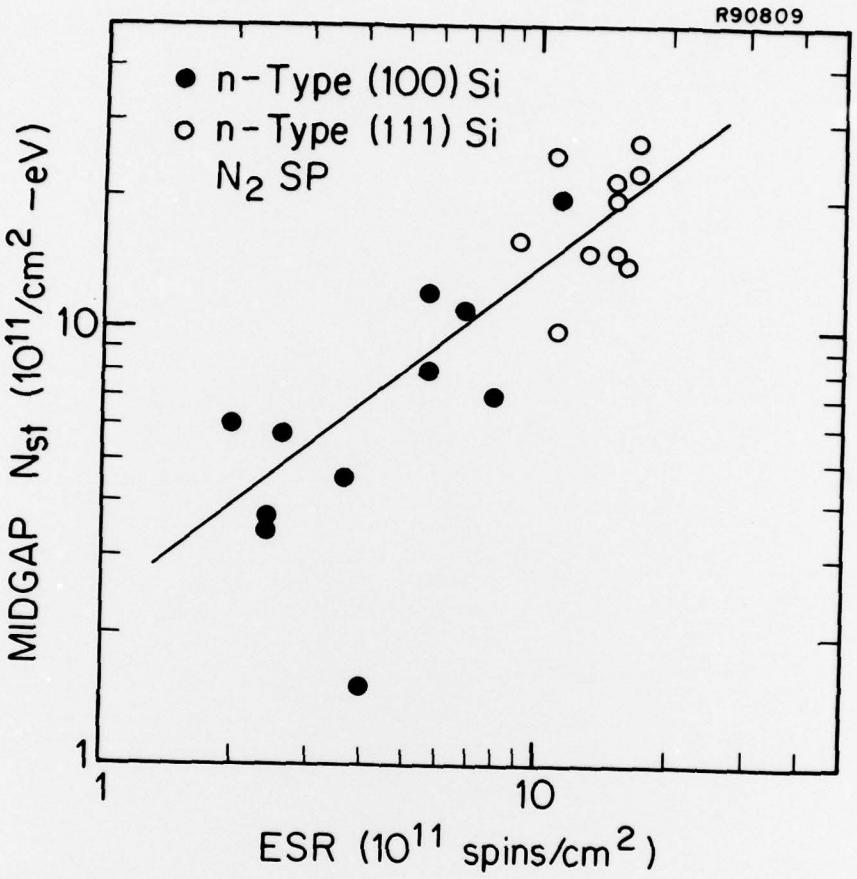

Fig. 4-4. Midgap interface state density (N_{st}) versus electron spin resonance (P_b) signals for n-type (100) and (111) wafers oxidized in dry O_2 at 800°, 1000°, and 1200°C and annealed/cooled in nitrogen. Wafers received no postoxidation hydrogen anneal.

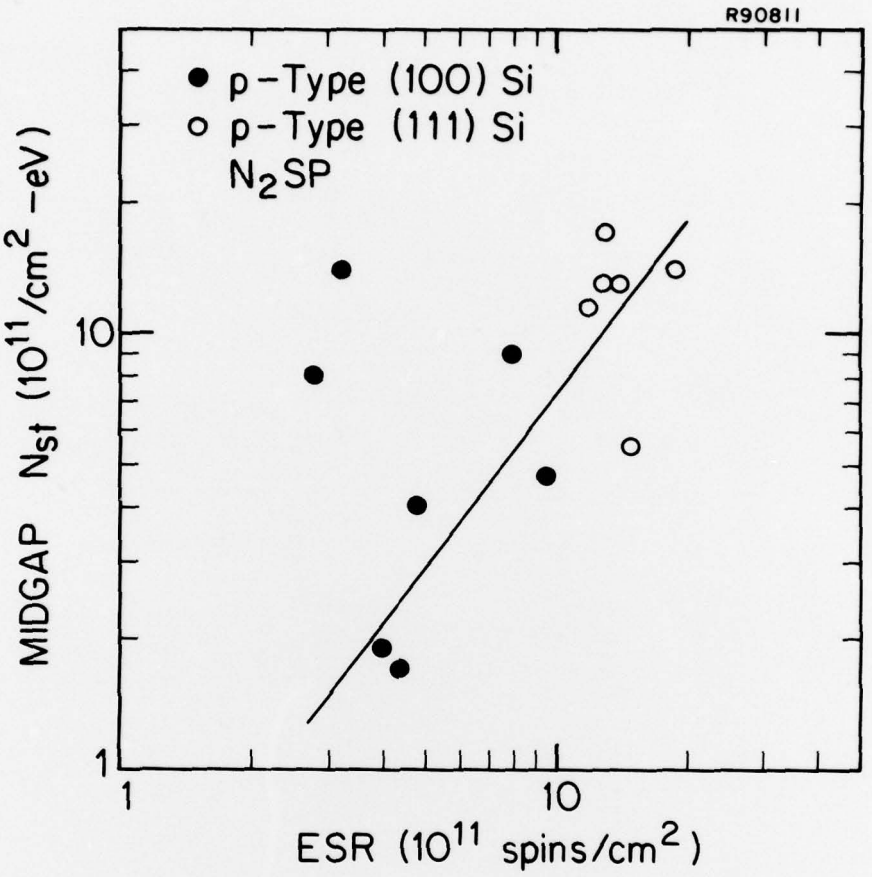

Fig. 4-5. Midgap interface state density (N_{st}) versus electron spin resonance (P_b) signals for p-type (100) and (111) wafers oxidized in dry O_2 at 1000° and 1200°C and annealed/cooled in nitrogen. Wafers received no post-oxidation hydrogen anneal.

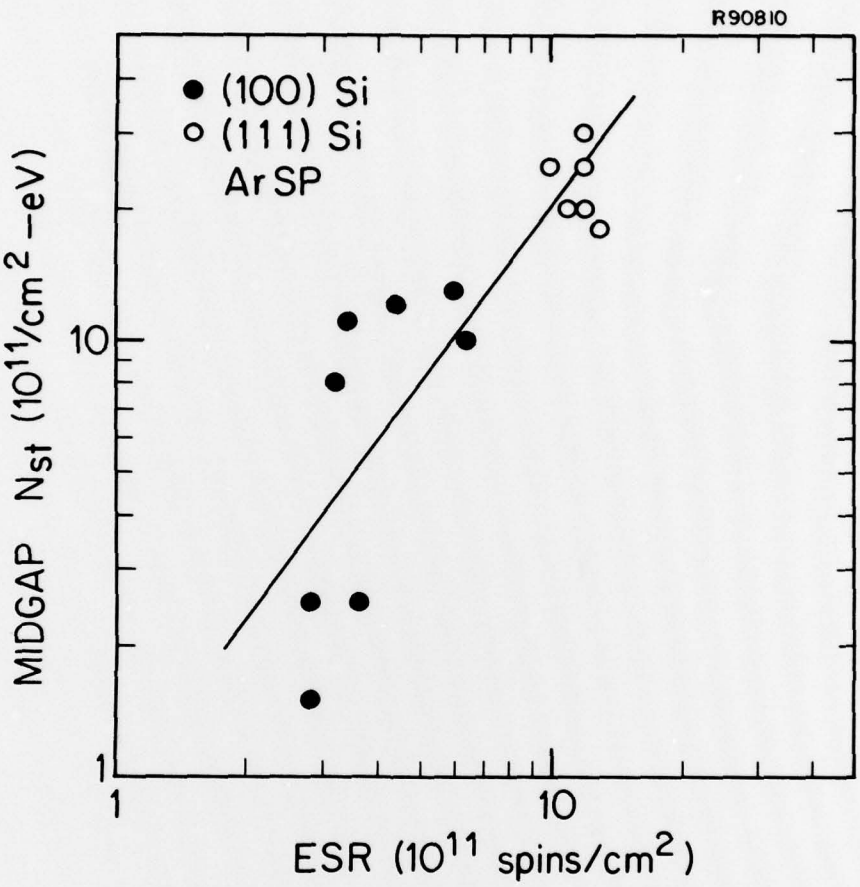

Fig. 4-6. Midgap interface state density (N_{st}) versus electron spin resonance (P_b) signals for n- and p-type (100) and (111) wafers oxidized in dry O_2 at 1000° and 1200°C and annealed/cooled in argon. Wafers received no post-oxidation hydrogen anneal.

condition. Application of a surface potential during the ESR measurement may result in different levels of P_b signals.

In conclusion, one of the important results of the investigation has been the observation of the correlation between ESR signals and interface state density levels at midgap, further evidence of which is also illustrated in Fig. 4-7. In this figure the effects of substrate dopants are illustrated. Very little change in either ESR or N_{st} values is observed for this range of resistivity. P_b signals were stronger for O_2FP samples and similarly N_{st} levels at midgap were higher. The exact nature of the relationship between N_{st} and P_b is still unclear and could be the topic of future work.

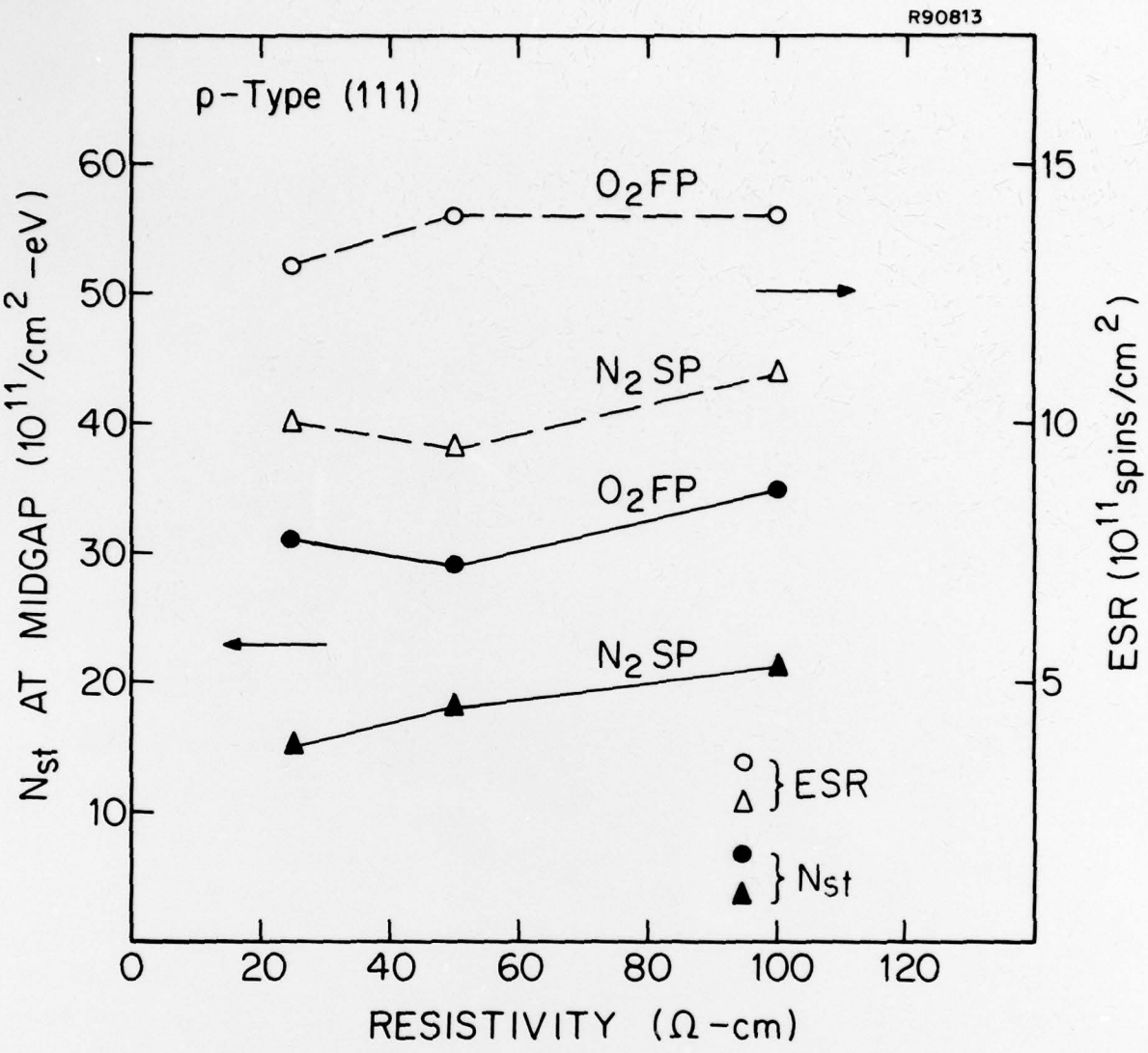

Fig. 4-7. Interface state density at midgap (N_{st}) and electron spin resonance (P_b) signals versus substrate resistivity for p-type (111) silicon wafers oxidized in dry O_2 at 1000°C and cooled either in the oxidizing ambient or in nitrogen following a 10 min in situ anneal.

5.0 SUMMARY AND CONCLUSIONS

Experiments have been completed which characterize the process dependence of fixed oxide charge (Q_{ss}), interface state density (N_{st}), and electron spin resonance signals (P_b). A relationship was established between fixed oxide charge and interface states prior to, as well as following, postoxidation hydrogen annealing. Likewise, a proportionality is observed for electron spin resonance data and interface states at midgap. The effect of oxide thickness, dopant type and concentration, and the incorporation of metallic impurities at the Si-SiO_2 interface were also investigated. The major conclusions from the program are summarized below:

(a) The silicon orientation effects commonly reported for both Q_{ss} and N_{st} have been observed. The ratios of Q_{ss} and N_{st} values (both unannealed and annealed) between (111) and (100) oriented silicon structures average slightly higher than 3:1.

(b) Ratios of N_{st} values between unannealed and hydrogen annealed samples are relatively constant for samples processed in oxygen and generally average 20:1.

(c) A basic difference in interface state density exists between samples pulled in an oxygen ambient, either fast pull or slow pull, and samples pulled in a nitrogen ambient. The latter seems to indicate the presence of both donor- and acceptor-like states while oxygen-pulled samples tend to indicate the absence of acceptor-like states.

(d) A proportionality exists between fixed charge density and interface state density for oxidized wafers which

did not receive a low-temperature postoxidation anneal in hydrogen. This proportionality is maintained in some cases after hydrogen annealing. In many cases the lowest achievable level of interface states seems dependent on the density of oxide fixed charge.

(e) Reintroduction of interface states by low-temperature nitrogen annealing is observed by the quasistatic technique and a corresponding increase in ESR signals is noted.

(f) The effect of p or n doping on P_b centers and N_{st} values at midgap are not found to be significant for substrate doping in the range 25-100 Ω-cm. Interface states are found to be inversely proportional with oxide thickness for postmetallization hydrogen anneal of dry O_2-pulled samples. No such dependence is noted prior to the anneal.

(g) Substantially weaker P_b signals were observed on (100) wafers as compared to (111), confirming earlier findings (9). This difference holds even though P_b (100) reflects a somewhat more complicated defect site structure (22).

(h) Strong evidence is obtained that a proportionality exists between ESR signals and midgap values of interface states. This relationship is dependent on wafer processing, particularly annealing and cooling ambients.

(i) The incorporation of iron at the Si-SiO_2 interface by ion implantation does not result in unusual interface state density distributions. Strong

silicon and SiO_2 damage ESR signals were confirmed in wafers implanted with no subsequent anneal. The damage signals are eliminated by anneal in 10% H_2 in N_2 at 1000°C. Implantation following oxidation results in stronger P_b signals and higher interface state density than in undisturbed oxides.

(j) The work reported here indicates that ESR is a significant tool in the characterization of the Si-SiO_2 system. It has the feature that it is applicable in certain cases where conventional techniques break down, e.g., very thin or thick oxides, or oxides with pinholes.

ACKNOWLEDGMENTS

The authors would like to thank Dr. J. F. Gibbons for providing the iron ion implantations, Julia Bien and Edward Dovichi for conducting various portions of the experimental work, and Drs. J. M. Early, E. H. Poindexter, and P. J. Caplan for critically reviewing the reports.

REFERENCES

(1) B. E. Deal and R. R. Razouk, Final Report No. ECOM-77-2665-F, June 1978, Contract No. DAAB07-77-C-2665.

(2) A. Goetzberger, E. Klausmann, and M. J. Schulz, CRC Crit. Rev. Solid-State Science, 6, 1 (1976).

(3) D. L. Griscom, J. Non-Crys. Solids, 24, 155 (1977).

(4) Y. C. Cheng, Prog. Surface Science, 8, 181 (1977).

(5) B. E. Deal, Proceedings of the Third International Symposium on Silicon Material Science and Technology, Electrochemical Society, Philadelphia, PA, May 8-13, 1977.

(6) B. E. Deal, M. Sklar, A. S. Grove, and E. H. Snow, J. Electrochem. Soc., 114, 266 (1967).

(7) R. Razouk and B. Deal, J. Electrochem. Soc., 126, 1573 (1979).

(8) E. Poindexter, P. Caplan, B. Deal, and R. Razouk, J. Appl. Phys., 50, 5847 (1979).

(9) E. H. Poindexter, E. R. Ahlstrom, and P. J. Caplan, in The Physics of SiO_2 and Its Interfaces, p. 227, Pergamon Press, NY (1978).

(10) E. H. Poindexter, J. N. Helbert, B. E. Wagner, and P. J. Caplan, IEEE Trans. Electron Devices, ED-24, 1217 (1977).

(11) M. Kuhn, Solid-State Electronics, 13, 873 (1970).

(12) R. Castagne and A. Vapaille, Surface Science, 28, 157 (1971).

(13) C. N. Berglund, IEEE Trans. Electron Devices, ED-13, 701 (1966).

(14) B. E. Deal, in "Semiconductor Silicon--1977," H. R. Huff and E. Sirtl, Editors, pp. 276-296, The Electrochemical Society, Inc., Princeton, NJ (1977).

(15) S. I. Raider, R. A. Gdula, and J. R. Petrak, Appl. Phys. Lett., 27, 150 (1975).

(16) E. Kooi, J. G. van Lierop, and J. A. Appels, J. Electrochem. Soc., 123, 1117 (1976).

(17) B. E. Deal and R. R. Razouk, Interim Report No. ECOM-78-0033-1, March 1979, Contract No. DAAG29-78-C-0033.

(18) Y. Nishi, Japan. J. Appl. Phys., 10, 82 (1971).

(19) P. J. Caplan, J. N. Helbert, B. E. Wagner, and E. H. Poindexter, Surface Science, 54, 33 (1976).

(20) T. Izumi and T. Matsumori, Japan. J. Appl. Phys., 14, 1067 (1975).

(21) Y. Nishi, Japan. J. Appl. Phys., 11, 85 (1972).

(22) E. H. Poindexter, P. J. Caplan, B. E. Deal, and R. R. Razouk, to be published.